frontiers | Frontiers in Chemistry

TYPE Original Research
PUBLISHED 25 August 2022
DOI 10.3389/fchem.2022.1003027

OPEN ACCESS

EDITED BY
Guangzhao Wang,
Yangtze Normal University, China

REVIEWED BY
Junli Chang,
Southwest University, China
Liu Xuefei,
Guizhou Normal University, China

*CORRESPONDENCE
Zishuang Cheng,
czs19950627@163.com
Chuntao Chang,
changct@dgut.edu.cn

SPECIALTY SECTION
This article was submitted to Theoretical and Computational Chemistry, a section of the journal Frontiers in Chemistry

RECEIVED 25 July 2022
ACCEPTED 03 August 2022
PUBLISHED 25 August 2022

CITATION
Wang F, Cheng Z, Zhang X, Xie C, Liu F, Chang C and Liu G (2022), A novel two-dimensional transition metal dichalcogenide as water splitting photocatalyst with excellent performances. *Front. Chem.* 10:1003027. doi: 10.3389/fchem.2022.1003027

A novel two-dimensional transition metal dichalcogenide as water splitting photocatalyst with excellent performances

Fang Wang[1,2], Zishuang Cheng[1,3]*, Xiaoming Zhang[3], Chunxiao Xie[1,4], Fucai Liu[2], Chuntao Chang[1]* and Guodong Liu[3]

[1]School of Mechanical Engineering, Neutron Scattering Technical Engineering Research Center, Dongguan University of Technology, Dongguan, China, [2]School of Optoelectronic Science and Engineering, University of Electronic Science and Technology of China, Chengdu, China, [3]School of Materials Science and Engineering, Hebei University of Technology, Tianjin, China, [4]Guangdong-Taiwan College of Industrial Science & Technology, Dongguan University of Technology, Dongguan, China

With the rising demand for renewable energy, photocatalysts are considered the most promising solution to harness solar energy, and the search for photocatalysts with excellent performances remains an urgent task. Here, based on density functional theory (DFT), the photocatalytic properties of $MoWS_4$ are systematically investigated. The $MoWS_4$ monolayer and bilayer are demonstrated as semiconductors with indirect band gaps of 2.01 and 1.48 eV. Moreover, they exhibit high and anisotropic light absorption coefficients of up to ~10^5 cm^{-1} in the visible-ultraviolet region. The intrinsic band edge positions could fully satisfy the redox potentials of water without any external adjustment. The electron mobility of $MoWS_4$ monolayer is 557 cm^2 $V^{-1}s^{-1}$, which is seven times higher than MoS_2 monolayer. Hence, $MoWS_4$ can be regarded as a promising 2D photocatalyst candidate for water splitting.

KEYWORDS

two-dimensional materials, transition metal dichalcogenides, water splitting photocatalyst, high mobility, density functional theory

Introduction

With the depletion of fossil energy and the increasing pollution of the natural environment, the demands for renewable energy become critical and urgent for sustainable development of global economy. In 1972, Fujishima and Honda discovered that TiO_2 can split water to produce hydrogen and oxygen in the presence of sunlight, making photocatalysis one of the most noteworthy solutions to harness solar energy (Fujishima and Honda, 1972). Afterwards, great efforts have been made to develop effective photocatalysts, including transition metal oxides, sulfides, nitrides, and so forth (Tsuji et al., 2005; Suntivich et al., 2011; Han et al., 2018). However, the low quantum efficiency derived from charge recombination on the surface and in the bulk of these

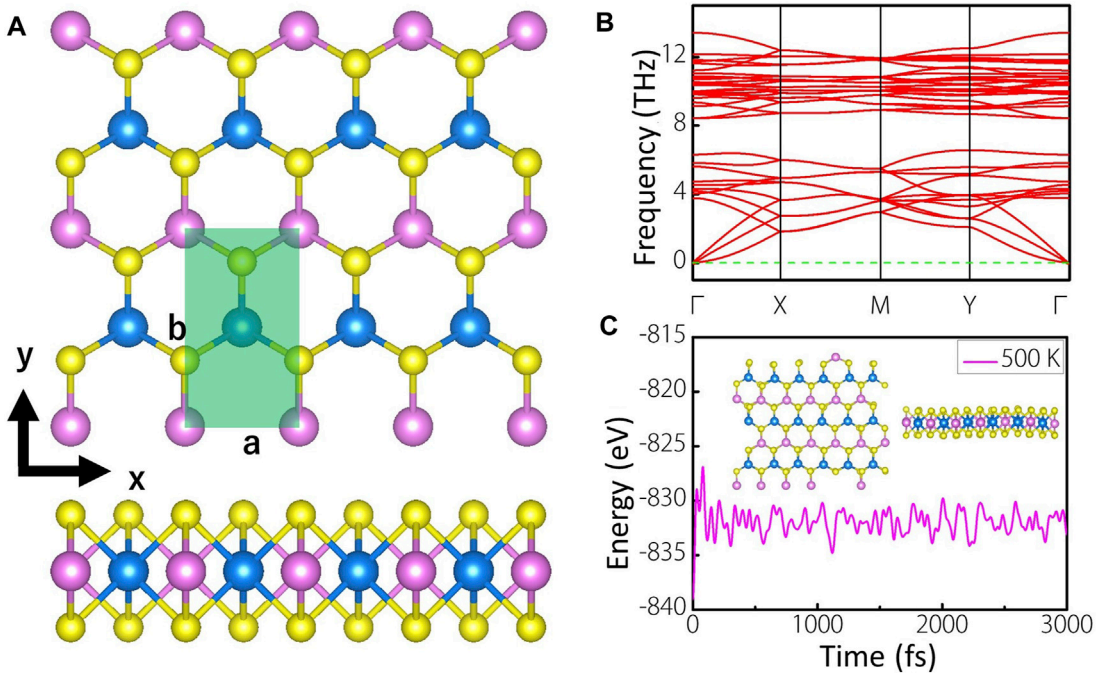

FIGURE 1
(A) Top and side views of $MoWS_4$ monolayer. The pink, blue, and yellow balls represent Mo, W, and S atoms, respectively. The light green area is the unit cell of $MoWS_4$ monolayer **(B)** Phonon spectra of $MoWS_4$ monolayer **(C)** Evolution of the total energy and a snapshot of $MoWS_4$ monolayer after a 3,000 fs AIMD simulations in vacuum at 500K

photocatalysts could not meet the criteria of favorable photocatalyst for sunlight driven water splitting (Fujishima et al., 2000).

Due to the interesting structures and corresponding electronic properties, two-dimensional (2D) materials have been widely used in various fields and also provide new research directions for efficient photocatalysis (Singh et al., 2015). In recent years, 2D photocatalysts showed the greater advantages over their bulk phase counterparts in terms of photocatalytic performance. For example, Both SnS_2 monolayer and ZnSe nanosheet exhibited higher photocurrent density than their bulk materials (Sun et al., 2012a; Sun et al., 2012b). In addition, various 2D materials have also been theoretically and experimentally demonstrated to be used as photocatalysts for water splitting, such as 2D transition metal dichalcogenides, g-C_3N_4, phosphorene, and so on (Wang et al., 2009; Zhuang and Hennig, 2013a; Rahman et al., 2016; Phuc et al., 2018; Zhang et al., 2022). However, few of these photocatalysts can simultaneously satisfy high visible light absorption, high carrier mobility and perfect band edge positions. For instance, MoS_2 monolayer showed lower carrier mobility, and $MoTe_2$ monolayer can't perfectly meet the redox potential of water (Wang et al., 2009; Zhuang and Hennig, 2013a; Cai et al., 2014; Rahman et al., 2016; Zhang et al., 2022). Both GaS and GaSe monolayers demonstrated low visible light absorption due to the large band gaps (Zhuang and Hennig, 2013b). Therefore, it is still a challenge to develop water splitting photocatalysts with excellent performances.

In this work, based on the first-principles calculations, we propose a novel 2D transition metal dichalcogenide namely $MoWS_4$ and systemically investigate its photocatalytic properties. Firstly, the stability of $MoWS_4$ monolayer is confirmed by calculating its phonon spectra and ab initio molecular dynamics (AIMD) simulations. Secondly, we calculate the band structures of $MoWS_4$ monolayer and bilayer, and show their semiconductive characteristic. Then, relevant photocatalytic properties are systematically investigated. It is found that $MoWS_4$ monolayer and bilayer can nicely meet the redox potentials without strain engineering, and their light absorption coefficients reach ~10^5 cm^{-1} in the visible-ultraviolet region. Moreover, the electronic mobility of $MoWS_4$ monolayer is as high as 557 cm^2 $V^{-1}s^{-1}$.

Computational details

For geometric and electronic structures, all calculations are performed by using the Vienna ab into simulation package (VASP) based on density functional theory (DFT) (Kresse and Furthmuller, 1996). We choose the generalized gradient

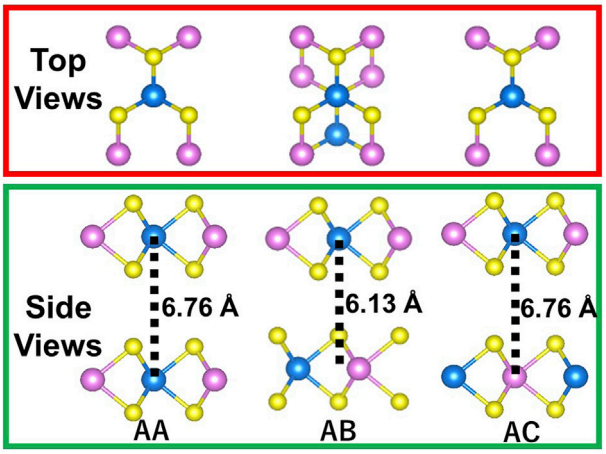

FIGURE 2
Top and side views of $MoWS_4$ bilayer with three stacking patterns (AA, AB, and AC).

approximation (GGA) of the Perdew–Burke–Ernzerhof (PBE) functional as the exchange-correlation functional to perform these calculations (Perdew et al., 1996). For the 2D monolayer structure, the vacuum layer thickness is set as about 20 Å to avoid layer-to-layer effects. The kinetic energy cutoff is set as 500 eV. The Brillouin zone is regulated with 10 × 6 × 1. During the calculations, the DFT-D2 method with Grimme correction is used to describe the long-range van der Waals interactions (Grimme, 2006). Besides, all atoms are fully relaxed, and the energy and force convergence criteria are set as 10^{-6} eV and 0.01 eV $Å^{-1}$, respectively. Except for PBE functional, to obtain the more accurate results, the HSE06 functional is also adopted to calculate the band structures and the band edge positions (Deák et al., 2010). To identify structural stability of $MoWS_4$ monolayer, its phonon spectra are calculated by using the PHONOPY code (Gonze and Lee, 1997). A 6 × 3 supercell structure of $MoWS_4$ monolayer is used in ab initio molecular dynamics (AIMD) simulations (NVT ensemble), which is carried out for 3 ps with a time step of 1 fs at 500 K (Cimas et al., 2014).

The optical properties can be defined by the complex dielectric function (frequency) for characterization:

$$\varepsilon(\omega) = \varepsilon_1(\omega) + i\varepsilon_2(\omega) \tag{1}$$

where $\varepsilon_1(\omega)$ and $\varepsilon_2(\omega)$ represent the real and imaginary parts, respectively. Based on the Kramers–Kronig transformation (Kuzmenko, 2005), the real part $[\varepsilon_1(\omega)]$ can be expressed as follows:

$$\varepsilon_1(\omega) = 1 + \left(\frac{2}{\pi}\right) p \int_0^{\infty} d\omega' \frac{\left(\omega'\right)^2 \varepsilon_2(\omega)}{\left(\omega'\right)^2 - (\omega)^2} \tag{2}$$

where p is the integral principal value. In addition, the imaginary part $[\varepsilon_2(\omega)]$ can be described as (Saha et al., 2000):

$$\varepsilon_2(\omega) = \frac{4\pi e^2}{m^2\omega^2} \sum_{i,f} \int \frac{2d^3k}{(2\pi)^3} \left|\langle ik|P|fk\rangle\right|^2 F_i^k\left(1 - F_f^k\right)\delta\left(E_f^k - E_i^k - E\right) \tag{3}$$

where ω, E, F, P, $||ik\rangle$, and $|fk\rangle$ represent the incident photon frequency, the incident photon energy, the Fermi function, the transition matrix, the CB state and VB state, respectively. Finally, the absorption coefficient $[\alpha(\omega)]$ can be calculated by (Cheng et al., 2022a):

$$\alpha(\omega) = \frac{\sqrt{2\omega}}{c}\left[\sqrt{\varepsilon_1^2(\omega) + \varepsilon_2^2(\omega)} - \varepsilon_1(\omega)\right]^{1/2} \tag{4}$$

where c denotes the speed of light in vacuum.

The carrier mobility is calculated by the following formula (Qiao et al., 2014):

$$\mu = \frac{e\hbar^3 C_{2D}}{k_B T m_e^* m_d E_d^2} \tag{5}$$

where C_{2D} is the elastic modulus, which can be expressed by $C_{2D} = \frac{1}{S_0}\frac{\partial^2 E}{\partial \delta^2}$, here E is the total energy of monolayer after deformation, S_0 is the lattice area of monolayer under equilibrium and δ is the uniaxial strain. Besides, k_B is the Boltzmann constant, T is the temperature. m_e^* is the effective mass along the transport direction and m_d is the average effective mass determined by $m_d = \sqrt{m_x^* m_y^*}$. E_d represents the deformation potential constant, which is expressed by $E_d = \frac{\partial E_{edge}}{\partial \delta}$, here E_{edge} represents the shift of the band edge position with respect to the uniaxial strain δ.

Results and discussions

Crystal structures, stability, and electronic properties

Figure 1A shows the top and side views of 4 × 2 supercell of $MoWS_4$ monolayer, which has a space group of *Pmm2*. The light green area is the unit cell of $MoWS_4$ monolayer, which contains four atoms. The pink, blue, and yellow balls represent Mo, W, and S atoms, respectively. $MoWS_4$ monolayer is a honeycomb structure from the top view, while sandwich structure from the side view, which is very similar to the structure of MoS_2 monolayer (Kan et al., 2014). After fully geometric optimization, the lattice constants are a = 3.188 Å and b = 5.526 Å with a layer thickness of 3.119 Å.

To confirm the stability of $MoWS_4$ monolayer, the formation energy (E_{form}), defined as: $E_{form} = [E_{MoWS_4} - E_{Mo} - E_W - 4E_S]/6$, is calculated, where E_{MoWS_4} presents the total energy of the unit cell of $MoWS_4$ monolayer, and E_{Mo}, E_W, and E_S present the energies of each Mo, W, and S atom in itself bulk phase, respectively. The calculated formation energy of $MoWS_4$ monolayer is −1.1 eV/atom (<0),

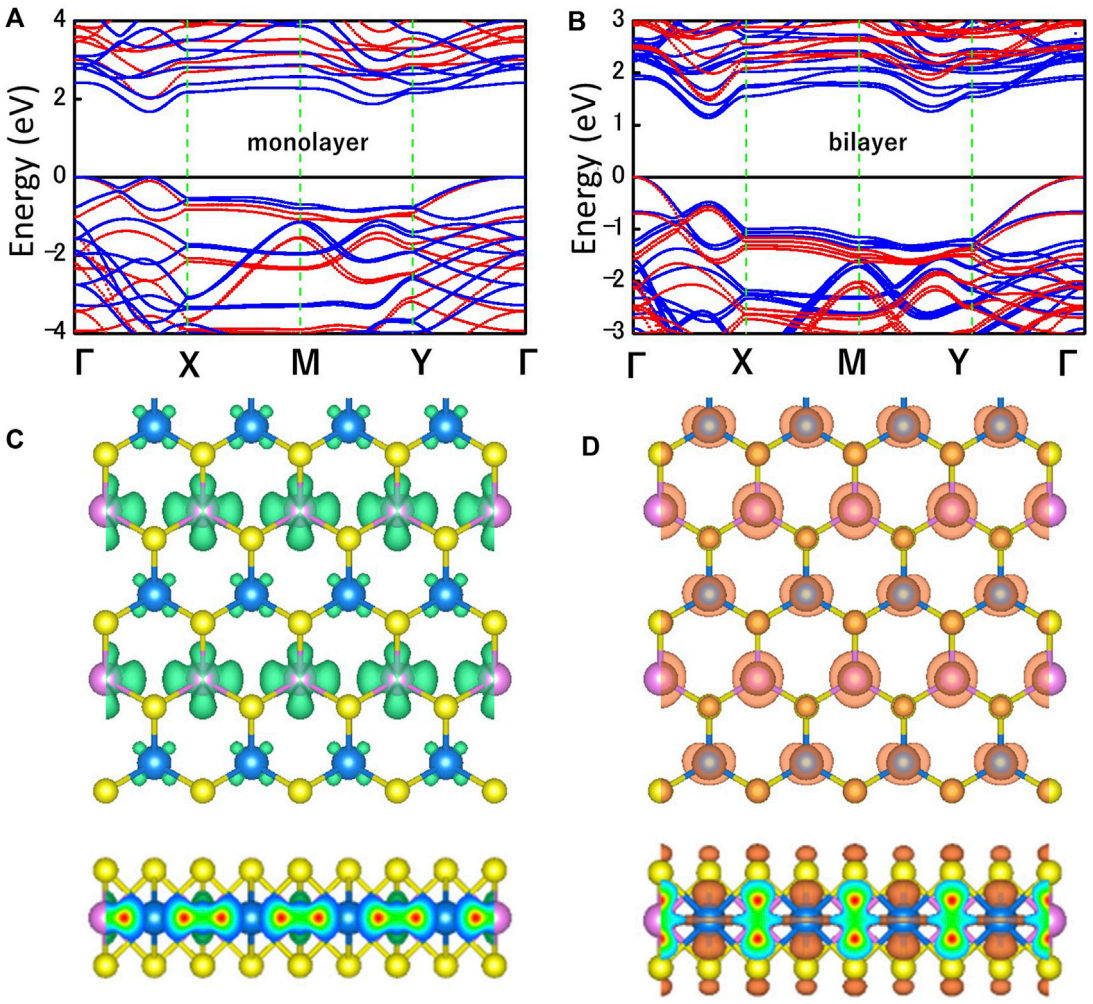

FIGURE 3
Band structures of **(A)** $MoWS_4$ monolayer and **(B)** $MoWS_4$ bilayer. The red and blue represent the HSE06 functional and PBE functional, respectively. Top and side views of the charge density at the **(C)** CBM, and **(D)** VBM. The isosurface value is set as 0.012 e $Å^{-3}$.

implying the procedure of synthesizing $MoWS_4$ monolayer is exothermic and favorable. Besides, the dynamic and thermal stabilities of $MoWS_4$ monolayer are further investigated. As shown in Figure 1B, the calculated phonon spectra exhibit no imaginary frequency, indicating high dynamic stability of $MoWS_4$ monolayer. The thermal stability is further studied *via* AIMD calculations. As illustrated in Figure 1C, the total energy of the $MoWS_4$ monolayer remains essentially stable and no deformation occurs in its final structure. These results suggest that $MoWS_4$ monolayer exhibits good dynamic and thermal stability, which deduces the possibility of experimental synthesis of $MoWS_4$ monolayer.

Figure 2 shows the top and side views of $MoWS_4$ bilayer. Three stacking patterns (AA, AB, and AC) are considered in the bilayer structures of $MoWS_4$. The results of the calculated total energy are −94.2727 eV, −94.4175 eV, and −94.2726 eV for AA, AB, and AC stacking patterns, respectively. AA and AC stacking structures have the same layer spacing of 6.76 Å, and AB stacking has a spacing of 6.13 Å. Obviously, the AB stacking structure is most stable energetically.

Figures 3A,B shows the electronic band structures of $MoWS_4$ monolayer and bilayer obtained by using the PBE functional (blue) and the HSE06 functional (red). The Fermi level and the high symmetry path are set as 0 eV and *Γ-X-M-Y-Γ*, respectively. The $MoWS_4$ monolayer and bilayer are indirect band gap semiconductors and their band gaps calculated by HSE06/PBE functional are 2.01/1.67 eV and 1.48/1.14 eV, respectively. The band gaps obtained by the HSE06 functional are larger than that obtained by the PBE functional since the PBE functional tends to underestimate the band gap. Figures 3C,D shows the maps of charge density for MoW_4 monolayer at the conduction band minimum (CBM) and the valence band maximum (VBM), and it

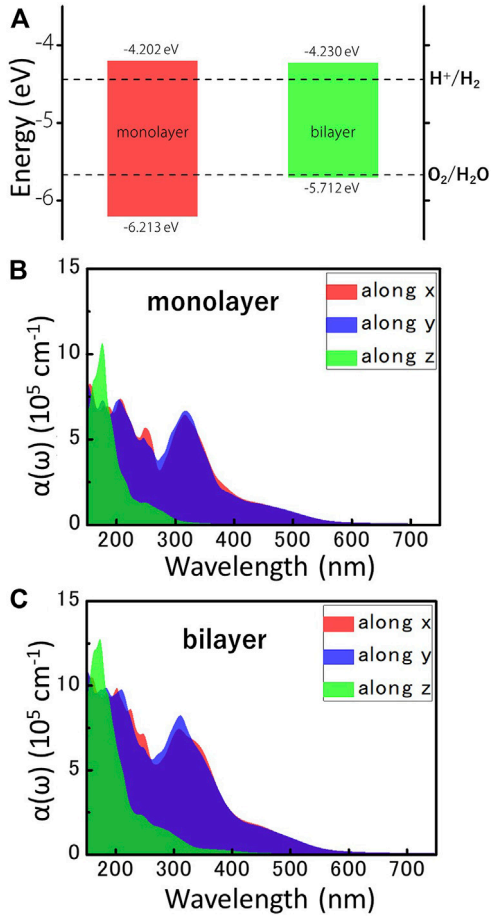

FIGURE 4
(A) The locations of VBM and CBM of $MoWS_4$ monolayer and bilayer, which are obtained by the HSE06 functional. The redox potentials of water splitting at pH = 0 are shown for comparison. All the energy levels are based on the vacuum level, and the vacuum level is set as 0 eV. The optical absorption coefficients for the different directions of **(B)** $MoWS_4$ monolayer and **(C)** $MoWS_4$ bilayer.

can be concluded that the CBM is mainly contributed by the Mo atoms, whereas the VBM comes from a combination of Mo, W, and S atoms.

Photocatalytic water splitting and optical properties

Considering the excellent semiconductor properties of $MoWS_4$ monolayer and bilayer, we systematically study their feasibility as photocatalysts for water splitting. It is well known that a photocatalytic candidate should meet the following conditions: Firstly, its band gap should exceed the free energy of water splitting (1.23 eV). Obviously, the band gaps of $MoWS_4$ monolayer and bilayer both exceed 1.23 eV; Secondly, its band edges must cross the redox potentials of water. The CBM energy should be higher than the reduction potential of H^+/H_2 (−4.44 eV), and the VBM energy should be lower than the oxidation potential of O_2/H_2O (−5.67 eV) (Abe, 2010; Sun et al., 2019; Cheng et al., 2022b). For 2D materials, the band edges with respect to the vacuum level ($E^{Vac}_{CBM/VBM}$) can be obtained by: $E^{Vac}_{CBM/VBM} = E^{DFT}_{CBM/VBM} - V_{vacuum}$, where $E^{DFT}_{CBM/VBM}$ represents the value of CBM/VBM obtain by DFT and V_{vacuum} represents the electrostatic potential in the vacuum region. We plot the map of band edges relative to the vacuum level of $MoWS_4$ monolayer and bilayer in Figure 4A, and find that the band edge positions of $MoWS_4$ monolayer and bilayer can perfectly satisfy the redox potential for the water splitting reaction at pH = 0. Specifically, the band edges of CBM/VBM for $MoWS_4$ monolayer and bilayer are −4.202/−6.213 eV and −4.230/−5.712 eV, respectively. Thus, the results suggest that the $MoWS_4$ monolayer and bilayer can be promising candidates for water splitting photocatalysts.

Besides, efficient light absorption is also an important feature for water splitting photocatalysts. Figures 4B,C shows the light absorption spectra of the $MoWS_4$ monolayer and bilayer within the visible-ultraviolet light range. The result can be summarized as follows: 1) Their light absorption coefficients in the ultraviolet light range are higher than visible light region (up to ~10^6 cm^{-1}); 2) Their light absorption coefficients of $MoWS_4$ bilayer overall are higher than that of $MoWS_4$ monolayer; 3) Their light absorption coefficients are significantly anisotropic: that is higher in the *z* direction, but have a wider range of light absorption spectra in the *x* and *y* directions. It is known that the high light absorption coefficients can guarantee the effective use of solar energy, which is very favorable for water splitting photocatalysts (Zhao et al., 2018; Fan et al., 2021). Therefore, both $MoWS_4$ monolayer and bilayer can be promising potential candidates as photocatalysts.

Strain engineering and high carrier mobility

We further investigate the effect of strain engineering on the photocatalytic performance of $MoWS_4$ monolayer. Figure 5 shows the band structures of $MoWS_4$ monolayer under the in-plane biaxial strain from −2 to 2%. Its band gap increases when compressive strain increases or tensile strain decreases, and its band gap varies in the range of 1.508–2.378 eV. In addition, when it is subjected to compressive strain, the indirect bandgap changes to be a direct bandgap; while when it is subjected to tensile strain, it remains an indirect bandgap semiconductor. As illustrated in Figure 6, we study the changes of its band edge positions under the applied in-plane biaxial strain. All of VBM positions are lower than the oxidation potential of O_2/H_2O under the −2~2% in-plane biaxial strain, which indicates that $MoWS_4$ monolayer always serves as a potential photocatalyst to generate

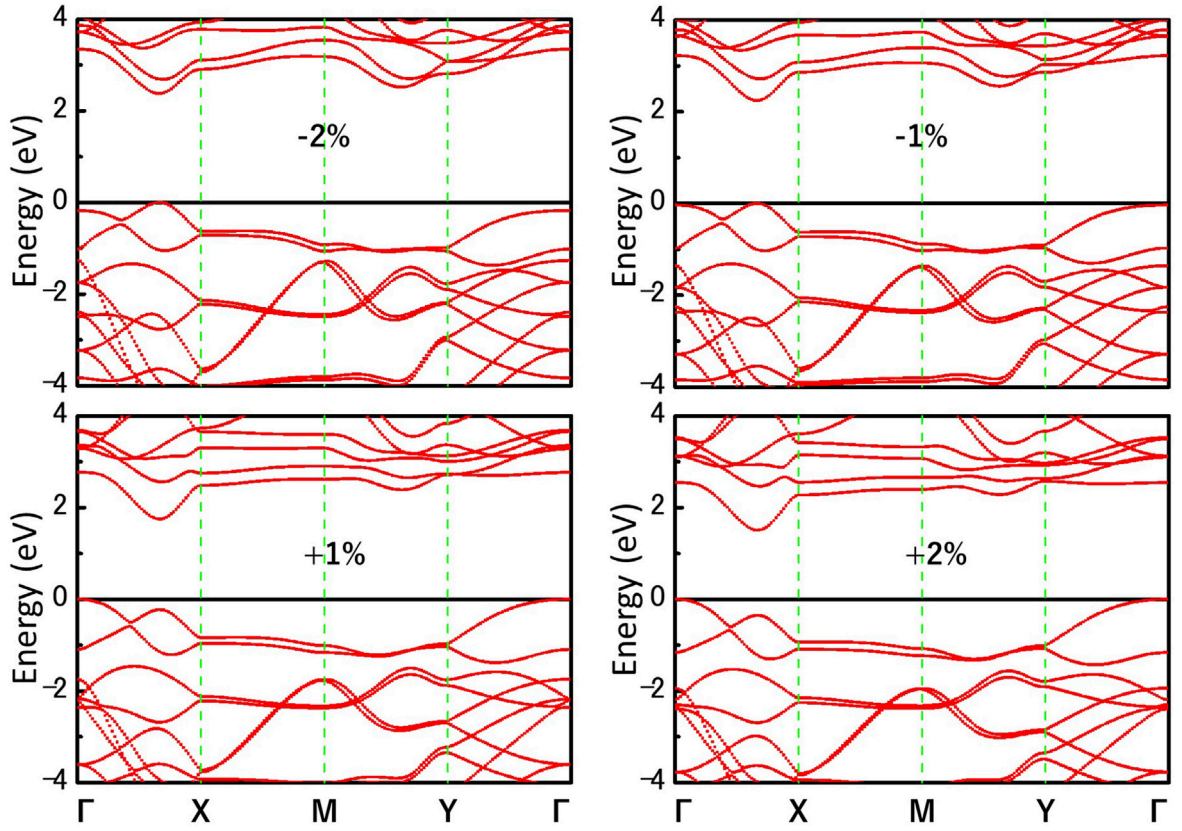

FIGURE 5
Band structures of $MoWS_4$ monolayer under the biaxial strain from −2 to 2% are calculated by HSE06 functional.

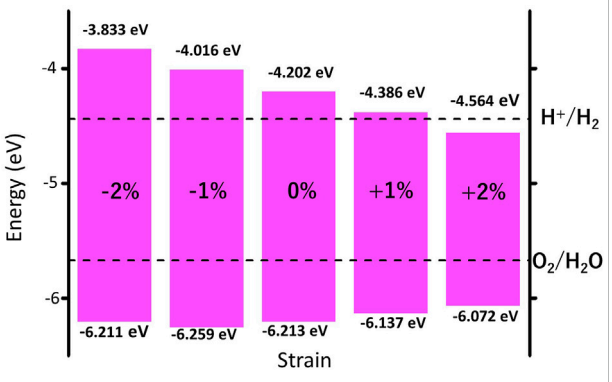

FIGURE 6
Strain effects on band edge positions of $MoWS_4$ monolayer with respect to the vacuum level (0 eV). The redox potentials of water splitting at pH = 0 are shown for comparison.

oxygen. Besides, when the applied tensile strain reaches 2%, its CBM positions become lower than the reduction potential of H^+/H_2. Thus, excessive tensile strain will lead to its inability to produce hydrogen. In general, compressive strain does not cause $MoWS_4$ monolayer to deviate from the basic requirements for water splitting photocatalyst, but tensile strain can easily affect its hydrogen production performance.

As we know, the fast carrier migration capability is necessary for high performance photocatalysts. Thus, the PBE functional is used to calculate the carrier mobility of $MoWS_4$ monolayer according to Eq. 5. Subsequently, we calculate its carrier effective masses (m^*), in-plane stiffness (C_{2D}) and deformation potential constants (E_d). Therein, to obtain E_d of $MoWS_4$ monolayer, the linear fitting maps of band edge positions are plotted as the function of the applied uniaxial strain δ along the x and y directions (Bardeen and Shockley, 1950; Zhang et al., 2021a), as illustrated in Figure 7 and the result is summarized in Table 1. It is notable that the values of E_d have a small difference along the x and y directions, which shows that the scattering ability of its carriers in different directions is also similar. In addition, the carrier effective masses of $MoWS_4$ monolayer have a small difference along the x and y directions. The electron effective masses of $MoWS_4$ monolayer are much lower than its hole effective masses ($m_e = 0.377m_0$ and $0.374m_0$ along the x and y directions), which are smaller than that of many 2D photocatalytic materials, such as Penta-PdSSe ($m_e = 2.16m_0$),

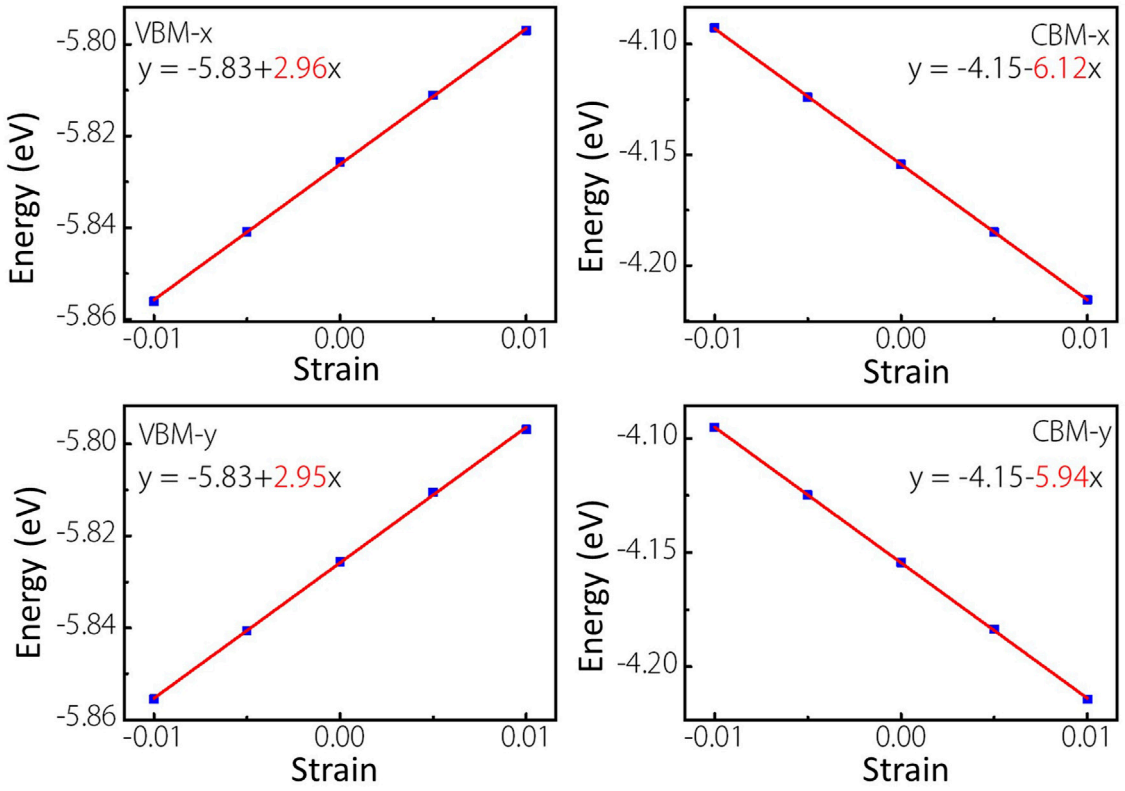

FIGURE 7
Linear fitting maps of VBM and CBM locations of $MoWS_4$ monolayer under the strain along *x* and *y* directions.

TABLE 1 Carrier effective masses m^*, In-plane stiffness C_{2D}, Deformation potential constants E_d, and carrier mobility μ for $MoWS_4$ monolayer along the *x* and *y* directions.

Materials	Direction	Carrier type	m^* (m_0)	C_{2D} (N/m)	E_d (eV)	μ ($cm^2V^{-1}s^{-1}$)
$MoWS_4$	*X*	Electron	0.377	131.86	6.12	529
		Hole	2.927	131.86	2.96	38
	Y	Electron	0.374	129.5	5.94	557
		Hole	2.857	129.5	2.95	38

Penta-$PdSe_2$ (m_e = 1.88m_0), δ-SnS (m_e = 1.01m_0), SnP_3 (m_e = 0.9m_0) (Long et al., 2018; Sun et al., 2018; Zhang et al., 2021b; Xiao et al., 2021). The smaller carrier effective masses benefit the transfer rate of photogenerated carriers in the photocatalytic process. What's more, the calculated electron mobility along *x* and *y* directions are 529 $cm^2V^{-1}s^{-1}$ and 557 $cm^2V^{-1}s^{-1}$, respectively, whereas the calculated hole mobility along *x* and *y* directions are both 38 $cm^2\ V^{-1}s^{-1}$. The reason for this difference is that the hole effective mass is much larger than the electron effective mass. More importantly, as shown in Figure 8, the electron mobility of $MoWS_4$ monolayer can significantly exceed that of many other 2D photocatalytic materials such as MoS_2 (μ_e = 72.16 $cm^2\ V^{-1}\ s^{-1}$, μ_h = 200.52 $cm^2\ V^{-1}\ s^{-1}$), Penta-PdS_2 (μ_e = 40.97 $cm^2\ V^{-1}\ s^{-1}$, μ_h = 339.25 $cm^2\ V^{-1}\ s^{-1}$), Penta-$PdSe_2$ (μ_e = 29.40 $cm^2\ V^{-1}\ s^{-1}$, μ_h = 534.55 $cm^2\ V^{-1}\ s^{-1}$), SnP_2S_6 monolayer (μ_e = 148.48 $cm^2\ V^{-1}\ s^{-1}$, μ_h = 143.12 $cm^2\ V^{-1}\ s^{-1}$), As_2S_3 monolayer (μ_e = 253.11 $cm^2\ V^{-1}\ s^{-1}$, μ_h = 10.85 $cm^2\ V^{-1}\ s^{-1}$) (Cai et al., 2014; Wang et al., 2015; Long et al., 2018; Jing et al., 2019; Liu et al., 2021). It is well known that materials with high carrier mobility can effectively reduce their photogenerated electron and hole recombination rates and increase the participation rate in redox reactions, which are beneficial for

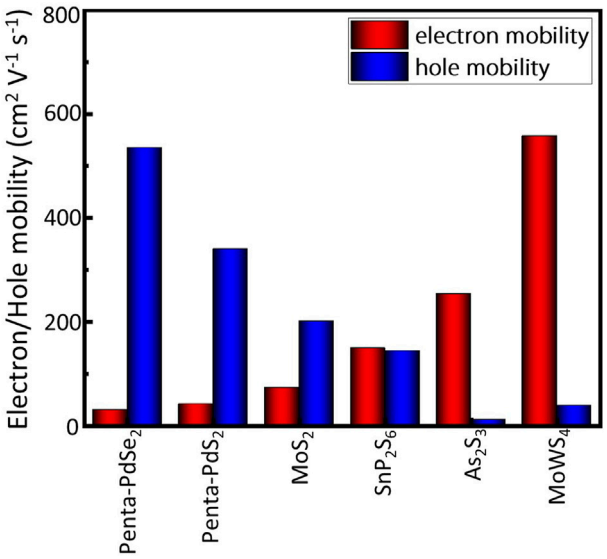

FIGURE 8
Carrier mobility of $MoWS_4$ compared with other typical 2D photocatalysts.

photocatalytic processes. Thus, our results suggest that $MoWS_4$ monolayer is a promising 2D photocatalyst candidate for water splitting.

Conclusion

Based on the first-principles calculations, we systematically investigate photocatalytic properties of two-dimensional $MoWS_4$. It is found that both the $MoWS_4$ monolayer and bilayer are semiconductors with indirect band gaps and show high and anisotropic light absorption coefficients in the visible-ultraviolet range. The band edge positions of the materials can satisfy the redox potentials perfectly and the electron mobility of $MoWS_4$ monolayer is up to 557 $cm^2 V^{-1} s^{-1}$, which outperforms many other 2D photocatalytic materials, such as MoS_2 monolayer, Penta-PdS_2, Penta-$PdSe_2$, and SnP_2S_6 monolayer. These results indicate that $MoWS_4$ can be a promising photocatalyst for water splitting with outstanding performances.

Data availability statement

The original contributions presented in the study are included in the article/Supplementary Material, further inquiries can be directed to the corresponding authors.

Author contributions

FW: Methodology, Investigation, Writing-original draft. ZC: Conceptualization, Investigation, Methodology, Writing—original draft. XZ: Investigation, Writing-original draft. CX: Validation, Resources. FL: Data curation, Validation. CC: Conceptualization, Writing—original draft, Supervision, Funding acquisition. GL: Validation, Data curation, Supervision.

Funding

The authors are grateful for support from the National Natural Science Foundation of China (52101192 and 51871056), Foundation for Basic and Applied Basic Research-Joint Foundation of Dongguan-Guangdong Province (2020A1515111109), and Department of Education of Guangdong in China (2018KZDXM069 and 2021 KCXTD050).

Conflict of interest

The authors declare that the research was conducted in the absence of any commercial or financial relationships that could be construed as a potential conflict of interest.

Publisher's note

All claims expressed in this article are solely those of the authors and do not necessarily represent those of their affiliated organizations, or those of the publisher, the editors and the reviewers. Any product that may be evaluated in this article, or claim that may be made by its manufacturer, is not guaranteed or endorsed by the publisher.

References

Abe, R. (2010). Recent progress on photocatalytic and photoelectrochemical water splitting under visible light irradiation. *J. Photochem. Photobiol. C Photochem. Rev.* 11, 179–209. doi:10.1016/j.jphotochemrev.2011.02.003

Bardeen, J., and Shockley, W. (1950). Deformation potentials and mobilities in non-polar crystals. *Phys. Rev.* 80, 72–80. doi:10.1103/physrev.80.72

Cai, Y. Q., Zhang, G., and Zhang, Y. W. (2014). Polarity-reversed robust carrier mobility in monolayer MoS_2 nanoribbons. *J. Am. Chem. Soc.* 136, 6269–6275. doi:10.1021/ja4109787

Cheng, Z. S., Zhang, X. M., Zhang, H., Liu, H. Y., Dai, X. F., Liu, G. D., et al. (2022). Binary pentagonal auxetic materials for photocatalysis and energy storage with outstanding performances. *Nanoscale* 14, 2041–2051. doi:10.1039/d1nr08368f

Cheng, Z. S., Zhang, X. M., Zhang, H., Liu, H. Y., Dai, X. F., Liu, G. D., et al. (2022). Two-dimensional auxetic pentagonal materials as water splitting photocatalysts with excellent performances. *J. Mat. Sci.* 57, 7667–7679. doi:10.1007/s10853-022-07130-x

Cimas, Á., Tielens, F., Sulpizi, M., Gaigeot, M. P., and Costa, D. (2014). The amorphous silica-liquid water interface studied by *ab initio* molecular dynamics (AIMD): Local organization in global disorder. *J. Phys. Condens. Matter* 26, 244106. doi:10.1088/0953-8984/26/24/244106

Deák, P., Aradi, B., Frauenheim, T., Janzén, E., and Gali, A. (2010). Accurate defect levels obtained from the HSE06 range-separated hybrid functional. *Phys. Rev. B* 81, 153203. doi:10.1103/physrevb.81.153203

Fan, Y. S., Xi, X. L., Liu, Y. S., Nie, Z. R., Zhao, L. Y., and Zhang, Q. H. (2021). Regulation of morphology and visible light-driven photocatalysis of WO_3 nanostructures by changing pH. *Rare Met.* 40, 1738–1745. doi:10.1007/s12598-020-01490-6

Fujishima, A., and Honda, K. (1972). Electrochemical photolysis of water at a semiconductor electrode. *Nature* 238, 37–38. doi:10.1038/238037a0

Fujishima, A., Rao, T. N., and Tryk, D. A. (2000). Titanium dioxide photocatalysis. *J. Photochem. Photobiol. C Photochem. Rev.* 1, 1–21. doi:10.1016/s1389-5567(00)00002-2

Gonze, X., and Lee, C. Y. (1997). Dynamical matrices, born effective charges, dielectric permittivity tensors, and interatomic force constants from density-functional perturbation theory. *Phys. Rev. B* 55, 10355–10368. doi:10.1103/physrevb.55.10355

Grimme, S. (2006). Semiempirical GGA-type density functional constructed with a long-range dispersion correction. *J. Comput. Chem.* 27, 1787–1799. doi:10.1002/jcc.20495

Han, N., Liu, P. Y., Jiang, J., Ai, L. H., Shao, Z. P., and Liu, S. M. (2018). Recent advances in nanostructured metal nitrides for water splitting. *J. Mat. Chem. A* 6, 19912–19933. doi:10.1039/c8ta06529b

Jing, Y., Zhou, Z. P., Zhang, J., Huang, C. B., Li, Y. F., and Wang, F. (2019). SnP_2S_6 monolayer: A promising 2D semiconductor for photocatalytic water splitting. *Phys. Chem. Chem. Phys.* 21, 21064–21069. doi:10.1039/c9cp04143e

Kan, M., Wang, J. Y., Li, X. W., Zhang, S. H., Li, Y. W., Kawazoe, Y., et al. (2014). Structures and phase transition of a MoS_2 monolayer. *J. Phys. Chem. C* 118, 1515–1522. doi:10.1021/jp4076355

Kresse, G., and Furthmuller, J. (1996). Efficient iterative schemes for *ab initio* total-energy calculations using a plane-wave basis set. *Phys. Rev. B* 54, 11169–11186. doi:10.1103/physrevb.54.11169

Kuzmenko, A. B. (2005). Kramers-Kronig constrained variational analysis of optical spectra. *Rev. Sci. Instrum.* 76, 083108. doi:10.1063/1.1979470

Liu, X. F., Zhang, Z. F., Ding, Z., Lv, B., Luo, Z. J., Wang, J. S., et al. (2021). Highly anisotropic electronic and mechanical properties of monolayer and bilayer As_2S_3. *Appl. Surf. Sci.* 542, 148665. doi:10.1016/j.apsusc.2020.148665

Long, C., Liang, Y., Jin, H., Huang, B. B., and Dai, Y. (2018). $PdSe_2$: Flexible two-dimensional transition metal dichalcogenides monolayer for water splitting photocatalyst with extremely low recombination rate. *ACS Appl. Energy Mat.* 2, 513–520. doi:10.1021/acsaem.8b01521

Perdew, J. P., Burke, K., and Ernzerhof, M. (1996). Generalized gradient approximation made simple. *Phys. Rev. Lett.* 77, 3865–3868. doi:10.1103/physrevlett.77.3865

Phuc, H. V., Hieu, N. N., Hoi, B. D., Hieu, N. V., Thu, T. V., Hung, N. M., et al. (2018). Tuning the electronic properties, effective mass and carrier mobility of MoS_2 monolayer by strain engineering: First-principle calculations. *J. Electron. Mat.* 47, 730–736. doi:10.1007/s11664-017-5843-8

Qiao, J. S., Kong, X. H., Hu, Z. X., Yang, F., and Ji, W. (2014). High-mobility transport anisotropy and linear dichroism in few-layer black phosphorus. *Nat. Commun.* 5, 4475–4477. doi:10.1038/ncomms5475

Rahman, M. Z., Kwong, C. W., Davey, K., and Qiao, S. Z. (2016). 2D phosphorene as a water splitting photocatalyst: Fundamentals to applications. *Energy Environ. Sci.* 9, 709–728. doi:10.1039/c5ee03732h

Saha, S., Sinha, T. P., and Mookerjee, A. (2000). Electronic structure, chemical bonding, and optical properties of paraelectric $BaTiO_3$. *Phys. Rev. B* 62, 8828–8834. doi:10.1103/physrevb.62.8828

Singh, A. K., Mathew, K., Zhuang, H. L., and Hennig, R. G. (2015). Computational screening of 2D materials for photocatalysis. *J. Phys. Chem. Lett.* 6, 1087–1098. doi:10.1021/jz502646d

Sun, Y. F., Cheng, H., Gao, S., Sun, Z. H., Li, Q. H., Liu, Q., et al. (2012). Freestanding tin disulfide single-layers realizing efficient visible-light water splitting. *Angew. Chem. Int. Ed. Engl.* 51, 8857–8861. doi:10.1002/ange.201204675

Sun, Y. F., Sun, Z. H., Gao, S., Cheng, H., Liu, Q. H., Piao, J. Y., et al. (2012). Fabrication of flexible and freestanding zinc chalcogenide single layers. *Nat. Commun.* 3, 1057–7. doi:10.1038/ncomms2066

Sun, S. S., Meng, F. C., Wang, H. Y., Wang, H., and Ni, Y. X. (2018). Novel two-dimensional semiconductor SnP_3: High stability, tunable bandgaps and high carrier mobility explored using first-principles calculations. *J. Mat. Chem. A* 6, 11890–11897. doi:10.1039/c8ta02494d

Sun, S. S., Meng, F. C., Xu, Y. F., He, J., Ni, Y. X., and Wang, H. Y. (2019). Flexible, auxetic and strain-tunable two dimensional penta-X_2C family as water splitting photocatalysts with high carrier mobility. *J. Mat. Chem. A* 7, 7791–7799. doi:10.1039/c8ta12405a

Suntivich, J., May, K. J., Gasteiger, H. A., Goodenough, J. B., and Yang, S. H. (2011). A perovskite oxide optimized for oxygen evolution catalysis from molecular orbital principles. *Science* 334, 1383–1385. doi:10.1126/science.1212858

Tsuji, I., Kato, H., and Kudo, A. (2005). Visible-light-induced H_2 evolution from an aqueous solution containing sulfide and sulfite over a ZnS-$CuInS_2$-$AgInS_2$ solid-solution photocatalyst. *Angew. Chem. Int. Ed. Engl.* 117, 3631–3634. doi:10.1002/ange.200500314

Wang, X. C., Maeda, K., Thomas, A., Takanabe, K., Xin, G., Carlsson, J. M., et al. (2009). A metal-free polymeric photocatalyst for hydrogen production from water under visible light. *Nat. Mat.* 8, 76–80. doi:10.1038/nmat2317

Wang, Y., Li, Y., and Chen, Z. F. (2015). Not your familiar two dimensional transition metal disulfide: Structural and electronic properties of the PdS_2 monolayer. *J. Mat. Chem. C* 3, 9603–9608. doi:10.1039/c5tc01345c

Xiao, F., Lei, W., Wang, W., Xu, L. L., Zhang, S. L., and Ming, X. (2021). Pentagonal two-dimensional noble-metal dichalcogenide PdSSe for photocatalytic water splitting with pronounced optical absorption and ultrahigh anisotropic carrier mobility. *J. Mat. Chem. C* 9, 7753–7764. doi:10.1039/d1tc01245b

Zhang, W., Chai, C. C., Fan, Q. Y., Sun, M. L., Song, Y. X., Yang, Y. T., et al. (2021). Two-dimensional tetrahex-GeC_2: A material with tunable electronic and optical properties combined with ultrahigh carrier mobility. *ACS Appl. Mat. Interfaces* 13, 14489–14496. doi:10.1021/acsami.0c23017

Zhang, Q., Wang, X., and Yang, S. L. (2021). δ-SnS: An emerging bidirectional auxetic direct semiconductor with desirable carrier mobility and high-performance catalytic behavior toward the water-splitting reaction. *ACS Appl. Mat. Interfaces* 13, 31934–31946. doi:10.1021/acsami.1c03650

Zhang, Y. F., Wei, J. M., Liu, T. Y., Zhong, Z., Luo, Z. J., Xiao, W. J., et al. (2022). Tunable properties of ZnSe/graphene heterostructure as a promising candidate for photo/electro-catalyst applications. *Appl. Surf. Sci.* 574, 151679. doi:10.1016/j.apsusc.2021.151679

Zhao, P., Ma, Y. D., Lv, X. S., Li, M. M., Huang, B. B., and Dai, Y. (2018). Two-dimensional III_2-VI_3 materials: Promising photocatalysts for overall water splitting under infrared light spectrum. *Nano Energy* 51, 533–538. doi:10.1016/j.nanoen.2018.07.010

Zhuang, H. L., and Hennig, R. G. (2013). Computational search for single-layer transition-metal dichalcogenide photocatalysts. *J. Phys. Chem. C* 117, 20440–20445. doi:10.1021/jp405808a

Zhuang, H. L., and Hennig, R. G. (2013). Single-layer group-III monochalcogenide photocatalysts for water splitting. *Chem. Mat.* 25, 3232–3238. doi:10.1021/cm401661x